Dynamics of populations and networks of neurons with voltage-activated and calcium-activated currents

Magnus J. E. Richardson*
Warwick Systems Biology Centre, University of Warwick, Coventry CV4 7AL, United Kingdom
(Received 3 April 2009; revised manuscript received 11 June 2009; published 24 August 2009)

The profile of transmembrane-channel expression in neurons is class dependent and a crucial determinant of neuronal dynamics. Here, a generalization of the experimentally verified exponential integrate-and-fire model is introduced that includes biophysical, nonlinear gated conductance-based currents, and a spike shape. A Fokker-Planck-based method is developed that allows for the rapid numerical calculation of steady-state and linear-response properties for recurrent networks of neurons with gating-variable dynamics slower than that of the voltage. This limit includes many cases of biological interest, particularly under *in vivo* conditions of high synaptic conductance. The utility of the method is illustrated by applying it to two biophysically detailed models adapted from the literature: an entorhinal layer-II cortical neuron and a neuron featuring both calcium-activated and voltage-activated spike-frequency-adaptation currents. The framework generalizes to networks comprised of different neuronal classes and so will allow for the modeling of emergent states in neural tissue at significantly increased levels of biological detail.

DOI: 10.1103/PhysRevE.80.021928 PACS number(s): 87.19.ll, 87.19.lc, 87.19.lq, 87.85.dm

I. INTRODUCTION

Low-dimensional models have been used from the outset to better understand the role of voltage-gated currents in neurons [1–3]. While initial reduced models focused on the continuous dynamics of action potentials, more recent contributions have replaced the spike with the discontinuous integrate-and-fire (IF) mechanism, freeing additional variables to capture properties of subthreshold or adaptation currents. Early forms of the latter models include the integrate-and-fire-or-burst model [4,5] with step activation and inactivation variables for the window calcium current I_T, a linearized resonate-and-fire model with a voltage threshold and a second-variable reset [6] and a multivariable generalized integrate-and-fire model that captured the effects of linearized subthreshold-activated currents [7,8]. Other reduced neuron models have examined effects of the high-threshold voltage-gated currents that lead to spike-frequency adaptation, typically treating a second variable as a spike counter with decay [9–11].

These early few-variable models featured a low threshold at the spike onset, around 10–20 mV from rest, of the leaky integrate-and-fire kind. However, it was demonstrated [12] through an analysis of a continuous-spike model [13] of the Hodgkin-Huxley form [14] that a significant improvement on the basic integrate-and-fire model is achieved by replacing the low threshold with an exponential runoff to capture the sodium-channel activation. This nonlinear exponential integrate-and-fire (EIF) model [12] has recently been shown experimentally to capture accurately the response properties of at least two classes of cortical neuron, specifically layer-five pyramidal cells [15] and fast spiking interneurons [16].

Around the same time as the development of the EIF, the two-variable Izhikevich model with a nonlinear quadratic spiking mechanism was introduced, featuring a second variable that captured phenomenologically both the effects of subthreshold and adaptation currents [17]. More recently, a related two-variable adaptive EIF (AdEx) model, with the quadratic spike replaced with an exponential spiking mechanism, has been proposed [18]. These models, although incorporating nonlinear spikes, approximate the gated conductances by a linear current-based second variable in common with the majority of previous studies.

In this paper generalized EIF model (GEM) neurons are introduced that feature an exponential EIF spike generation [12] with arbitrary spike shape and conductance-based gated currents with nonlinear voltage-activation profiles and time constants. It will be demonstrated that both steady-state and first-order dynamical properties can be derived for a range of biophysically meaningful cases in which the dynamics of the gating variables are long compared to those of the voltage. The approach uses the threshold integration method, developed for the efficient numerical solution to nonlinear IF models [19,20] and allows for the first-order response to arbitrarily patterned afferent synaptic conductance input to be derived for both populations and networks of neurons. It will be further demonstrated that the discontinuous spiking mechanism of the integrate-and-fire class of models can be smoothed by adding a spike shape that may be matched to experiment. The framework therefore increases significantly the range of biological details that can be incorporated into reduced neuron models while still retaining solvability.

The paper is structured as follows. in Sec. II the general form of the model is defined. Section III demonstrates how to derive the steady-state properties of a population of GEM neurons that feature, as an example, a slow depolarization-activated hyperpolarizing current, and in Sec. IV the first-order dynamics of a population of the same neurons is derived. In Sec. V a recurrent network of GEM neurons with filtered delayed inhibitory conductance is examined. Finally, Sec. VI illustrates the application of the method to two biophysically detailed models adapted from the literature. The Appendixes contain details for the implementation of the

*Corresponding author; magnus.richardson@warwick.ac.uk

threshold integration method and the extension of the method to neurons with a spike shape.

II. DEFINITION OF THE MODEL

The membrane voltage V of an electrotonically compact neuron of capacitance C obeys a current-balance equation

$$C\frac{dV}{dt} + I_{ion} = I_{syn}, \tag{1}$$

where I_{ion} is the summed ionic currents and I_{syn} is the synaptic current. The latter is treated in the Gaussian approximation in which the tonic and the modulated components of the excitatory and the inhibitory synaptic conductances $g_e(t)$ and $g_i(t)$ are retained but in which fluctuations are approximated by a stochastic current (conductance fluctuations, however, can be easily included; see Ref. [19]). The synaptic current therefore takes the form

$$I_{syn} = g_e(E_e - V) + g_i(E_i - V) + g_L\sigma\sqrt{2C/g_L}\xi(t), \tag{2}$$

where $E_e=0$ mV and $E_i=-70$ mV are the reversal potentials of excitation and inhibition. The fluctuation strength is parametrized by the constant σ which, because of the leak conductance g_L (see below) included in the fluctuation term, has units of voltage. In this paper dynamics of the fluctuation strength σ [21–23] are not considered but, again, may be easily addressed using the methods of Ref. [19]. The quantity $\xi(t)$ is a Gaussian white noise process with zero mean and a Dirac-delta autocorrelation $\langle\xi(t)\xi(t')\rangle=\delta(t-t')$.

Writing $I_e=g_e(E_e-V)$ for the nonfluctuating excitatory component of the synaptic current (and similarly for inhibition I_i) gives the combined nonfluctuating component as

$$I_s = I_e + I_i = g_s(E_s - V), \tag{3}$$

$$g_s = g_e + g_i, \quad E_s = \frac{g_eE_e + g_iE_i}{g_s}. \tag{4}$$

In this paper the steady-state synaptic current will often be parametrized by g_{s0} and E_{s0} (the 0 subscript will always be used to denote a steady-state quantity). If the underlying excitatory g_{e0} and inhibitory g_{i0} conductances are required, then these can be re-expressed in terms of the g_{s0}, E_{s0} parameters

$$g_{e0} = g_{s0}\frac{E_{s0} - E_i}{E_e - E_i}, \quad g_{i0} = g_{s0}\frac{E_{s0} - E_e}{E_i - E_e} \tag{5}$$

from inverting the relations in equation pair (4).

Generalized EIF Models — GEMs

A GEM model with a single gating variable will be used as an example in this paper (for Figs. 1–3 and 5). The ionic current has three terms $I_{ion}=I_L+I_{spike}+I_x$. The leak current takes the standard form $I_L=g_L(V-E_L)$. The spike-generating current I_{spike} is modeled here using the experimentally verified [15] exponential IF [12] approximation

$$I_{spike} = -g_L\Delta_T e^{(V-V_T)/\Delta_T} \tag{6}$$

with V_T as the voltage at which the current begins to activate and Δ_T parametrizing the rapidity at onset. The potassium-mediated resetting of the spike is modeled by a threshold at V_{th} followed by a reset to V_{re}. The reset need not be instantaneous and in a later section it will be shown that a fixed spike shape and refractory period may be incorporated into the framework. The third component of the ionic current is a slow voltage-activated current $I_x=g_xx(V-E_x)$ with a gating variable $x(t)$ obeying a filter equation governed by a voltage-dependent time constant $\tau_x(V)$ and equilibrium value $x_\infty(V)$. Combining all these terms for the ionic and the synaptic currents yields

$$C\frac{dV}{dt} = g_L(E_L - V) + g_L\Delta_T e^{(V-V_T)/\Delta_T} + g_xx(E_x - V) + g_s(E_s - V) + g_L\sigma\sqrt{2C/g_L}\xi(t), \tag{7}$$

$$\tau_x\frac{dx}{dt} = x_\infty - x \tag{8}$$

with a threshold at V_{th} and a reset at V_{re} completing the dynamics. Equations (7) and (8) for the voltage and the gating variable represent a two-dimensional system of coupled stochastic differential equations. For the example model a parameter choice is made in which $x_\infty(V)$ is depolarization activated and the current is hyperpolarizing, providing negative feedback. The values of all parameters are provided in Appendix C. An example of the evolution of $V(t)$ and $x(t)$ given by Eqs. (7) and (8) is plotted in Fig. 1(A) and the voltage dependence of τ_x and x_∞ can be seen in Fig. 1(B).

III. POPULATIONS OF NEURONS IN THE STEADY STATE

Equations (7) and (8) for state variables V and x are stochastic and so it is convenient to move to a probabilistic representation in which the dynamics of the probability distribution $P(V,x,t)$ is considered. The system is fully described by a one-plus-two-dimensional Fokker-Planck equation [24] which, unfortunately, does not appear to be solvable in closed form. The strategy used in this paper is to consider cases for which the gating-variable dynamics are long compared to the time scales in the voltage dynamics. This approach has been taken previously for two-variable linearized models [7,8,11] and, as will be seen, covers a range of biophysically meaningful cases in the context of nonlinear models.

Under these long-time-constant conditions, the steady-state distribution of the gating variable will be strongly peaked at a particular value. This can be seen in a simulational example for Eqs. (7) and (8) in Fig. 1(A). By replacing the dynamics of the gating variable $x(t)$ with its average x_0, the steady-state probability density can be reduced to a function of voltage only $P_0(V;x_0)$ with x_0 acting as a parameter. The steady-state gating x_0 can be extracted from the model using a self-consistent approach: it will first be demonstrated how x_0 can be found if the probability density $P_0(V;x_0)$ is

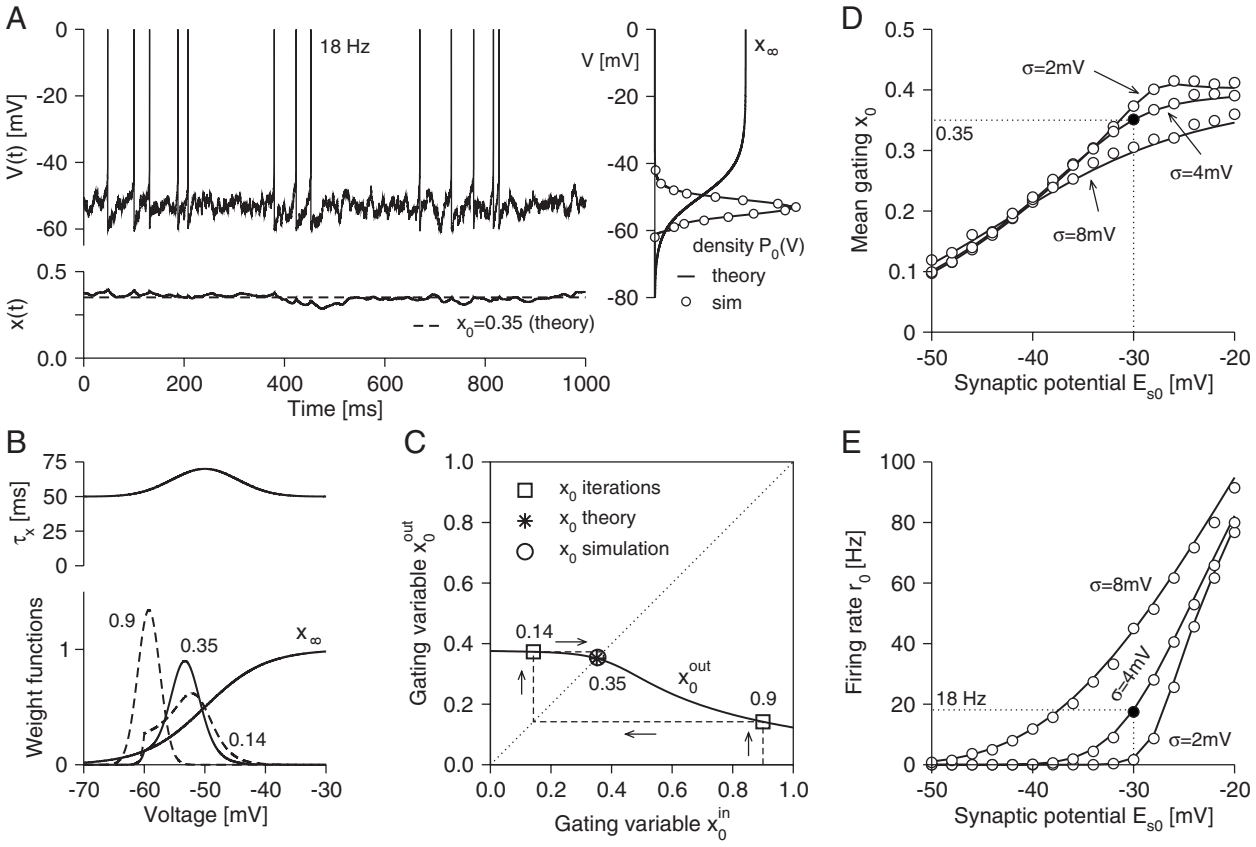

FIG. 1. Steady-state properties of a generalized EIF Model (GEM) with a nonlinear depolarization-activated hyperpolarizing current. (A)–(C) Example with a tonic synaptic drive $g_{s0}=2g_L$, $E_{s0}=-30$ mV ($g_{e0}=1.14g_L$, $g_{i0}=0.86g_L$), and fluctuations $\sigma=4$ mV. (A) Voltage $V(t)$ and gating variable $x(t)$ [simulations of Eqs. (7) and (8)] with average firing rate of ~18 Hz for the simulations. The probability density (circles, simulation) is shown in the inset together with $x_\infty(V)$. (B) Voltage profiles of $\tau_x(V)$ and $x_\infty(V)$ shown with examples of the weighting function $P_0(V;x_0^{in})/\tau_x(V)$ for $x_0^{in}=0.14,0.35,0.9$. (C) Two schemes for finding x_0. Solid line shows x_0^{out} [Eq. (17)] for the full range $x_0^{in}=0\rightarrow 1$ with the intersection $x_0^{out}=x_0^{in}=0.35$ giving the self-consistent solution. This is identical to the simulational average (circle) to two decimal places. An alternative iterative scheme [dashed line, Eq. (18)] is also shown, with the first two points (squares, $x_0^{in}=0.9,0.14$) and fixed point (star, five iterations $x_0^{in}=0.35$). These values were used for the example weighting functions of panel (B). The theoretical probability density $P_0(V;x_0=0.35)$ is plotted in the inset of panel (A) and agrees well with the simulation (circles) with the theoretical steady-state rate $r_0=18.1$ Hz also close to the simulational value. (D) Steady-state gating variable x_0 [solutions of Eq. (17)] and (E) corresponding firing rates [Eqs. (15) and (16)] for a range of E_{s0} with fixed $g_{s0}=2g_L$. Theory (lines) and simulation (symbols) are compared for three fluctuation strengths σ. Filled symbols correspond to the example in panels (A)–(C). Other model parameters are provided in Appendix C.

known, and second how the probability density $P(V;x_0)$ can be calculated if x_0 is known. These two results will then be combined and solved simultaneously.

A. Mean gating from the voltage distribution

An equation for the mean gating variable x_0 as a function of the steady-state voltage distribution will now be derived using a heuristic argument (a formal derivation is also possible from the full Fokker-Planck equation following the method used in a related problem [8]). A steady state is considered in which, due to the fluctuations in voltage, the gating variable $x(t)=x_0+x_F(t)$ is fluctuating around some mean value x_0. If the time constant $\tau_x(V)$ is longer than the correlation time in the voltage dynamics, the fluctuations $x_F(t)$ will tend to average out and therefore will be suppressed. Substitution into Eq. (8) yields

$$\frac{dx_F}{dt}=\frac{x_\infty(V)-x_0-x_F}{\tau_x(V)}. \tag{9}$$

τ_x has been brought into the denominator of the right-hand side (RHS) because a steady-state average is sought and there would otherwise have been a contribution from the strong correlation between τ_x and the rate of change in x_F. With this step taken, it is now possible to take the steady-state average of both sides of Eq. (9). This yields

$$0=\left\langle\frac{x_\infty}{\tau_x}\right\rangle_0-x_0\left\langle\frac{1}{\tau_x}\right\rangle_0-\left\langle\frac{x_F}{\tau_x}\right\rangle_0, \tag{10}$$

where the notation $\langle\psi\rangle_0$ implies the average of the voltage-dependent quantity ψ over the steady-state voltage distribution $P(V;x_0)$. The last term in Eq. (10) which contains the average over x_F can be neglected as less significant because in the long-time-constant limit fluctuations in x are sup-

pressed. Rearranging the remaining terms gives the steady-state average of the gating variable as

$$x_0 \simeq \frac{\langle x_\infty/\tau_x\rangle_0}{\langle 1/\tau_x\rangle_0}, \tag{11}$$

which is identical to a result of Ref. [9] derived in a related case of spike-frequency adaptation. Equation (11) gives the mean steady-state gating in terms of a weighted average of $x_\infty(V)$ with respect to $P_0(V;x_0)/\tau_x(V)$. This comprises the initially unknown probability density $P_0(V,x_0)$, which is itself a function of x_0. It will now be demonstrated how this probability density may be found if x_0 is known.

B. Voltage distribution from the mean gating

The approximation made is that the gating variable is sharply peaked around its average value x_0, so that $x(t)$ may be replaced with x_0 in Eq. (7). This reduces the dynamics of the two-variable neuron model to a standard one-dimensional exponential integrate-and-fire model [12] which is solvable. Calling the steady-state firing rate r_0, the continuity equation [19,24] for the steady-state probability flux J_0 obeys

$$\frac{dJ_0}{dV} = r_0[\delta(V - V_{re}) - \delta(V - V_{th})], \tag{12}$$

where the Dirac delta functions ensure that the flux of trajectories taken out at threshold are reinserted at the reset. In the steady state the equation for the flux itself takes the form

$$-CJ_0 = I_0 P_0 + g_L\sigma^2\frac{\partial P_0}{\partial V}, \tag{13}$$

where I_0 is the summed ionic and nonstochastic component of the synaptic currents I_{s0} [Eq. (3)]

$$I_0 = g_L(V - E_L) + g_L\Delta_T e^{(V-V_T)/\Delta_T} + g_x x_0(V - E_x) + g_{s0}(V - E_{s0}). \tag{14}$$

The gradient in the probability density (diffusive term) in Eq. (13) arises from the stochastic component of the synaptic current, proportional to σ in Eq. (2).

Equations (12) and (13) fully specify the steady-state distribution in terms of the firing rate r_0. A convenient method of solution for these equations that also generalizes to the later time-dependent case is the threshold integration method [19,20]. Because both J_0 and P_0 in Eqs. (12) and (13) scale linearly with the (initially unknown) steady-state rate r_0, it can be scaled out by introducing $J_0 = r_0 j_0$, $P_0 = r_0 p_0$, so that the equations become

$$-\frac{\partial j_0}{\partial V} = -\delta(V - V_{re}), \tag{15}$$

$$-\frac{\partial p_0}{\partial V} = \frac{I_0}{g_L\sigma^2}p_0 + \frac{C}{g_L\sigma^2}j_0, \tag{16}$$

where the conditions at V_{th} are $j_0(V_{th})=1$ and $p_0(V_{th})=0$. These equations can now be solved numerically by discretizing the voltage range and by integrating backward from threshold V_{th} to some lower bound V_{lb} (the exact value of which is unimportant as long as it is below a value where neuronal voltages are typically found). The steady-state firing rate is then recovered from the condition $r_0 = 1/\int_{V_{lb}}^{V_{th}} dV\, p_0(V)$, which in turn yields the correctly normalized probability density $P_0 = r_0 p_0$. Details of a convenient numerical scheme are provided in Appendix A.

C. Self-consistent solution for the steady state

Equation (11) gives the steady-state gating if the probability density $P_0(V;x_0)$ is known, whereas the solutions to Eqs. (15) and (16) conversely give the probability density if the steady-state gating x_0 in the current I_0 of Eq. (14) is known. These equations can be solved together by treating x_0 as a parameter in Eqs. (15) and (16), scanning over its range $x_0 = 0 \to 1$ and identifying the self-consistent solutions where Eq. (11) is satisfied, i.e., when $x_0^{out} = x_0^{in}$ in

$$x_0^{out} = \frac{\int_{-\infty}^{\infty} dV\, P_0(V,x_0^{in})x_\infty(V)/\tau_x(V)}{\int_{-\infty}^{\infty} dV\, P_0(V,x_0^{in})/\tau_x(V)}. \tag{17}$$

This procedure is illustrated in Figs. 1(B) and 1(C) (solid line). In Fig. 1(B) the weight functions $P_0(V;x_0)/\tau_x(V)$ for three examples of x_0 are plotted together with $x_\infty(V)$ and $\tau_x(V)$ profiles. In Fig. 1(C) the x_0^{out} of Eq. (17) is plotted over the range of x_0^{in} (solid line). A single fixed point is seen at the intersection of x_0^{out} with $x_0^{out} = x_0^{in}$ (dotted line) giving the self-consistent solution $x_0 = 0.35$. The corresponding probability density $P_0(V;x_0)$ is compared with simulation in the inset of Fig. 1(A). Figures 1(D) and 1(E) show the results for the steady-state gating x_0 and firing rate r_0 over a range of synaptic potentials E_{s0} for three different synaptic fluctuation strengths. For this particular model the hyperpolarizing gated current has a significant effect on the steady-state firing rate. For example, for a standard EIF model (i.e., with $g_x = 0$), the steady-state rate for $E_{s0} = -30$ mV, $\sigma = 4$ mV would have been 88 Hz rather than 18 Hz [filled symbol, Fig. 1(E)].

It is worth noting that an iterative method is often a rather convenient alternative approach to finding the steady states, particularly if there is more than one gating variable. This involves inserting an initial guess $x_0^{in(1)}$ into the RHS of Eq. (17) to generate a new estimate $x_0^{in(2)} = x_0^{out}(x_0^{in(1)})$, etc. This is repeated m times until the convergence

$$x_0^{in(m)} \to x_0 \tag{18}$$

is considered satisfactory. An example of this procedure is also shown in Fig. 1(C). In certain cases a damped iteration method is preferable in which the new value is combined with a weighted sum of the previous value

$$x_0^{in(k+1)} = \alpha x_0^{out}(x_0^{in(k)}) + (1 - \alpha)x_0^{in(k)} \tag{19}$$

with α chosen in the range $0 \to 1$ at some value appropriate for convergence.

D. Richness of GEM dynamics

The analytical framework developed in this paper is applicable to a subset of GEM neurons, i.e., those with slowly

gated currents receiving stochastic synaptic drive that, at the population level, has a single steady-state firing rate. Unrestricted GEM neurons, however, share much of the dynamical richness of conductance-based models with continuous Hodgkin-Huxley-like spikes. For example, for the deterministic case, it is known that feedback from gated currents can yield type II behavior and bistability [8] and, even in the presence of fluctuations, neurons are not guaranteed to have a steady state; instabilities can arise from the interactions of the voltage distribution with the gating-variable activation profile to yield spontaneous subthreshold oscillations or bursting. GEM neurons share the rich dynamics of continuous conductance-based models, but their discontinuous spike renders them considerably more tractable. So, although beyond the scope of this paper, it is worth noting that the GEM framework should allow for analytical headway to be made on the collective properties of neurons with more complex dynamics.

IV. POPULATION RESPONSE TO MODULATION

Once the steady-state distribution has been approximated, it is relatively straightforward to extract the corresponding first-order response to temporally patterned synaptic drive. A scenario is first considered in which excitatory synaptic conductance $g_e(t)=g_{e0}+\hat{g}_{e1}e^{i\omega t}$ is modulated at a frequency $\omega/2\pi$. From Eq. (3)

$$I_s = I_{s0} + \hat{I}_{s1}e^{i\omega t} = g_{s0}(E_{s0}-V) + \hat{g}_{e1}(E_e - V)e^{i\omega t}. \quad (20)$$

To a first-order approximation, this will induce sinusoidal oscillations at the same frequency in the instantaneous firing rate and probability density

$$r \simeq r_0 + \hat{r}_1 e^{i\omega t}, \quad (21)$$

$$P \simeq P_0 + \hat{P}_1 e^{i\omega t}. \quad (22)$$

The aim will be to extract the first-order dynamics perturbatively from the Fokker-Planck equation, with the steady state being the zeroth order. In general the density P is a function of both V and x. However, in the long-time-constant approximation fluctuations of $x(t)$ are suppressed and the dynamics of $x(t)$ for a single neuron can be expected to follow $x(t) \simeq x_0+\hat{x}_1 e^{i\omega t}$ on average. In this limit the modulated probability density can be well approximated as being a function of voltage only $\hat{P}_1(V;\hat{x}_1)$ but parametrized by the (initially unknown) gating-variable modulation $\hat{x}_1$.

The next two sections follow a similar approach to that taken for the steady state: first an approximation for $\hat{x}_1$ will be derived in terms of the modulated density $\hat{P}_1(V;\hat{x}_1)$, and second the modulated density will be derived as a function of $\hat{x}_1$. These results will yield simultaneous equations that can be solved to give the first-order response to an arbitrarily patterned synaptic drive.

A. Modulated gating from the distribution

The gating-variable dynamics of a single neuron under modulation can be written as $x(t)=x_0+\hat{x}_1 e^{i\omega t}+x_F$, where $\hat{x}_1$ is the (complex) amplitude of the induced modulation and x_F are fluctuations around these values. Substitution into the gating equation (8) gives

$$\frac{dx_F}{dt} = \frac{x_\infty - x_0}{\tau_x} - \hat{x}_1\left(\frac{1}{\tau_x} + i\omega\right)e^{i\omega t} - \frac{x_F}{\tau_x}. \quad (23)$$

Taking the average of this equation over the probability density in Eq. (22), while neglecting the less significant fluctuating terms containing averages over x_F, yields an equation for the first-order modulation of the gating variable

$$\hat{x}_1 \simeq \frac{\langle x_\infty/\tau_x\rangle_1 - x_0\langle 1/\tau_x\rangle_1}{\langle 1/\tau_x\rangle_0 + i\omega}, \quad (24)$$

where $\langle\psi\rangle_1$ is shorthand for the integral of $\psi(V)\hat{P}_1$ over the voltage range $V_{lb}\rightarrow V_{th}$ and where $\langle\psi\rangle_0$ is the steady-state expectation of $\psi(V)$. Equation (24) gives $\hat{x}_1$ as a function of the initially unknown density $\hat{P}_1(V;\hat{x}_1)$.

B. Modulated distribution from the gating

The method for finding $\hat{P}_1(V;\hat{x}_1)$ is equivalent to calculating the first-order response properties of the standard exponential integrate-and-fire neuron. This problem is solved [19] and is achieved using a threshold integration method similar to the steady-state case. The starting points are the time-dependent continuity equation

$$\frac{\partial P}{\partial t} + \frac{\partial J}{\partial V} = r(t)[\delta(V-V_{re}) - \delta(V-V_{th})] \quad (25)$$

and flux equation

$$-CJ = (I_{ion} - I_s)P + g_L\sigma^2\frac{\partial P}{\partial V}. \quad (26)$$

The modulated flux $J(V,t)=J_0(V)+\hat{J}_1(V)e^{i\omega t}$ and all other relevant quantities are now substituted into Eqs. (25) and (26) and terms at first order in the modulations are retained. The substitution $x=x_0+\hat{x}_1 e^{i\omega t}$ in I_x inside I_{ion} is also made. This yields the following pair of differential equations:

$$-\frac{\partial \hat{J}_1}{\partial V} = i\omega\hat{P}_1 + \hat{r}_1[\delta(V-V_{th}) - \delta(V-V_{re})], \quad (27)$$

$$-\frac{\partial \hat{P}_1}{\partial V} = \frac{I_0}{g_L\sigma^2}\hat{P}_1 + \frac{C}{g_L\sigma^2}\hat{J}_1 + \frac{g_x\hat{x}_1}{g_L}\frac{(V-E_x)}{\sigma^2}P_0 + \frac{\hat{g}_{e1}}{g_L}\frac{(V-E_e)}{\sigma^2}P_0, \quad (28)$$

which can be compared with the steady-state case (15) and (16). Note that in Eq. (28) there are two inhomogeneous components proportional to P_0. The first term has a prefactor $g_x\hat{x}_1$ (where $\hat{x}_1$ is initially unknown) and represents the induced modulation of the voltage-activated current by the second term, with prefactor $\hat{g}_{e1}$, which is the modulated excitatory synaptic drive.

Because Eq. (28) is linear in $g_x\hat{x}_1$ and $\hat{g}_{e1}$, these quantities can be scaled out by first solving Eqs. (27) and (28) with

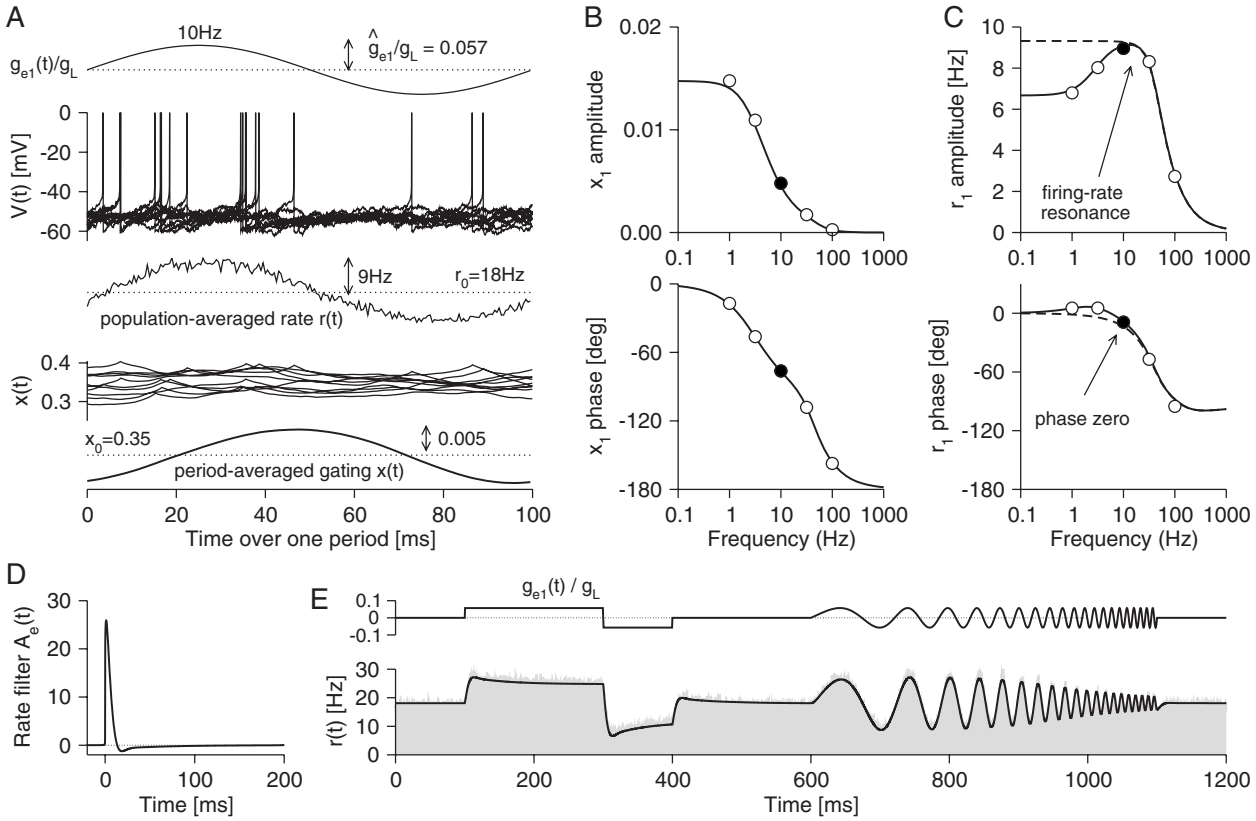

FIG. 2. Response of a population of GEM neurons to modulated synaptic conductance. (A) Simulations of voltage, population-averaged rate, gating-variable, and period-averaged gating-variable for a sinusoidally modulated excitatory conductance $g_{e1}=0.057g_L$ at a frequency of 10 Hz [all other parameters are shared with the steady-state example in panels (A)–(C) of Fig. 1]. (B) Amplitude and phase of the modulated gating $\hat{x}_1$ [solid line, theory (42); symbols, simulation; filled symbol 10 Hz example of panel (A)]. (C) Corresponding amplitude and phase of the firing-rate modulation [Eq. (38)]. A firing-rate resonance at ~13 Hz and phase zero at ~5 Hz are visible, but absent in the rate modulation of an equivalent neuron with no gating-variable dynamics [dashed lines, Eq. (38) with $\gamma_x=0$]. (D) The firing-rate filter $A_e(t)$ for excitatory synaptic conductance modulation derived from inverse Fourier transforming $r_1(\omega)$ [see Eq. (44)]. The negative tail is characteristic of the slow negative feedback generated by this particular voltage-activated current. (E) Population response to patterned excitatory synaptic drive [solid line, theory Eq. (45); gray histogram, simulations]. Note the sag or overshoot response to step changes in conductance. Parameters not provided in the caption to Fig. 1 can be found in Appendix C.

each inhomogeneous term separately and then appropriately combining the two solutions. Introducing the dimensionless conductances $\hat{\gamma}_{e1}=\hat{g}_{e1}/g_L$ and similarly for g_x, we can write the probability density as $\hat{P}_1=\gamma_x\hat{x}_1\hat{P}_x+\hat{\gamma}_{e1}\hat{P}_e$ (and analogously for $\hat{J}_1$ and $\hat{r}_1$), where the quantities $\hat{P}_x,\hat{J}_x,\hat{r}_x$ and $\hat{P}_e,\hat{J}_e,\hat{r}_e$ satisfy equations of the form

$$-\frac{\partial\hat{J}_\mu}{\partial V}=i\omega\hat{P}_\mu+\hat{r}_\mu[\delta(V-V_{th})-\delta(V-V_{re})], \tag{29}$$

$$-\frac{\partial\hat{P}_\mu}{\partial V}=\frac{I_0}{g_L\sigma^2}\hat{P}_\mu+\frac{C}{g_L\sigma^2}\hat{J}_\mu+\frac{(V-E_\mu)}{\sigma^2}P_0 \tag{30}$$

with $\mu=e$ or $\mu=x$ fixing the appropriate reversal potential in the inhomogeneous term of Eq. (30). Equations of this form are readily solved [19] by the threshold integration method by first resolving the quantities $\hat{J}_\mu$ and $\hat{P}_\mu$ into two parts

$$\hat{J}_\mu=\hat{J}_\mu+\hat{r}_\mu\hat{J}_r,\quad \hat{P}_\mu=\hat{p}_\mu+\hat{r}_\mu\hat{p}_r. \tag{31}$$

The pair $\hat{J}_\mu,\hat{p}_\mu$ addresses the inhomogeneous component proportional to $(V-E_\mu)P_0$ and satisfy the equations

$$-\frac{\partial\hat{J}_\mu}{\partial V}=i\omega\hat{p}_\mu, \tag{32}$$

$$-\frac{\partial\hat{p}_\mu}{\partial V}=\frac{I_0}{g_L\sigma^2}\hat{p}_\mu+\frac{C}{g_L\sigma^2}\hat{J}_\mu+\frac{(V-E_\mu)}{\sigma^2}P_0 \tag{33}$$

with boundary conditions $\hat{J}_\mu(V_{th})=0$, $\hat{p}_\mu(V_{th})=0$. The pair and $\hat{J}_r,\hat{p}_r$ address the firing threshold at V_{th} and the reset V_{re} and satisfy the equations

$$-\frac{\partial\hat{J}_r}{\partial V}=i\omega\hat{p}_r-\delta(V-V_{re}), \tag{34}$$

$$-\frac{\partial \hat{p}_r}{\partial V} = \frac{I_0}{g_L\sigma^2}\hat{p}_r + \frac{C}{g_L\sigma^2}\hat{J}_r \tag{35}$$

with boundary conditions $\hat{J}_r(V_{th})=1$ [which takes care of the delta function at V_{th} present in Eq. (29)] and $\hat{p}_r(V_{th})=0$. The pairs of Eqs. (32) and (33) and Eqs. (34) and (35) can be integrated from threshold to the lower bound V_{lb} using the same integration scheme used for the steady state. The unknown modulation amplitude $\hat{r}_\mu$ in Eq. (31) is then extracted from the requirement that the flux vanishes at the lower bound $\hat{J}_\mu(V_{lb})=0$, so that

$$0 = \hat{J}_\mu(V_{lb}) + \hat{r}_\mu \hat{J}_r(V_{lb}), \tag{36}$$

$$\hat{r}_\mu = -\hat{J}_\mu(V_{lb})/\hat{J}_r(V_{lb}). \tag{37}$$

Although the lower bound V_{lb} appears in the fixing of $\hat{r}_\mu$, its exact value has no significant effect on the result if it is chosen to be sufficiently hyperpolarized.

Result (37) for $\hat{r}_\mu$ can now be used, together with equation set (31) to yield the functions $\hat{J}_\mu$ and $\hat{P}_\mu$. Together, these give the total probability density and the firing rate

$$\hat{r}_1 = \gamma_x \hat{x}_1 \hat{r}_x + \hat{\gamma}_{e1}\hat{r}_e, \tag{38}$$

$$\hat{P}_1 = \gamma_x \hat{x}_1 \hat{P}_x + \hat{\gamma}_{e1}\hat{P}_e \tag{39}$$

in terms of $\hat{x}_1$.

C. Self-consistent solution for modulations

Equation (24) for $\hat{x}_1$ and Eq. (39) for $\hat{P}_1(V;\hat{x}_1)$ can now be solved simultaneously. Multiplying the density $\hat{P}_1$ in Eq. (39) separately by x_∞/τ_x and $1/\tau_x$ and integrating over the voltage range yields

$$\langle x_\infty/\tau_x\rangle_1 = \gamma_x \hat{x}_1 \langle x_\infty/\tau_x\rangle_x + \hat{\gamma}_{e1}\langle x_\infty/\tau_x\rangle_e, \tag{40}$$

$$\langle 1/\tau_x\rangle_1 = \gamma_x \hat{x}_1 \langle 1/\tau_x\rangle_x + \hat{\gamma}_{e1}\langle 1/\tau_x\rangle_e \tag{41}$$

with $\langle\psi\rangle_\mu$ as the integral $\psi\hat{P}_\mu$ from $V_{lb}\to V_{th}$. Substituting these two equations into result (24) and rearranging gives the solution for the modulated amplitude as $\hat{x}_1=\hat{\gamma}_{e1}\hat{x}_{e1}$, where

$$\hat{x}_{e1} = \frac{\langle x_\infty/\tau_x\rangle_e - x_0\langle 1/\tau_x\rangle_e}{\langle 1/\tau_x\rangle_0 + i\omega - \gamma_x(\langle x_\infty/\tau_x\rangle_x - x_0\langle 1/\tau_x\rangle_x)}. \tag{42}$$

From this result the modulated density $\hat{P}_1$ and the firing rate $\hat{r}_1$ follow directly from Eqs. (38) and (39).

The results of this procedure are illustrated in Fig. 2 for a modulation of the excitatory synaptic conductance around the steady-state case of Figs. 1(A)–1(C). In Fig. 2(A) simulation time courses of the voltage and the gating variable are provided for a modulation frequency of 10 Hz. The population rate and the gating variable averaged across periods are also shown with the amplitudes marked. Figure 2(B) shows the amplitude and the phase of the modulated gating variable $\hat{x}_1$ from Eq. (42) for a range of frequencies. The corresponding firing-rate modulation amplitude and phase appears in Fig. 2(C). A firing-rate resonance and phase zero are visible, as expected [7] for a neuron with a voltage-activated current that leads to slow negative feedback. In the absence of the voltage-gated channel the modulation would be $\hat{r}_1=\hat{\gamma}_{e1}\hat{r}_e$ [from setting $\gamma_x=0$ in Eq. (38) for the rate modulation]. This is also plotted in Fig. 2(C) (dashed line) and exhibits neither a firing-rate resonance nor a phase zero. Finally, it can be noted that even for this relatively high level of modulation [$\max(\hat{r}_1)/r_0 \simeq 9$ Hz/18 Hz=50%] agreement between simulations and the first-order approximation is close.

D. Response to patterned synaptic drive

The rate response $\hat{r}_1(\omega)$ due to oscillatory synaptic drive at frequency $\omega/2\pi$ can be used to derive the first-order response to arbitrary synaptic-conductance wave forms $g_{e1}(t)$. Scaling out the implicit amplitude $\hat{\gamma}_{e1}$ in Eq. (38) gives a frequency-dependent filter

$$\tilde{A}_e(\omega) = \frac{\hat{r}_1(\omega)}{\hat{\gamma}_{e1}} = \gamma_x \hat{x}_{e1}\hat{r}_x + \hat{r}_e. \tag{43}$$

The inverse Fourier transform of which is the time-dependent filter for the response to excitatory conductance change

$$A_e(t) = \int_{-\infty}^{\infty} \frac{d\omega}{2\pi}\tilde{A}_e(\omega)e^{i\omega t}. \tag{44}$$

An example of this filter is plotted in Fig. 2(D) calculated from the inverse transform of the rate modulation in Fig. 2(C). Note that after the initial peak an extended negative tail is visible. The filter $A_e(t)$ can be used to calculate the firing-rate response to arbitrary drive via the convolution

$$r(t) = r_0 + \int_{-\infty}^{\infty} dt\, A_e(t-t')g_{e1}(t')/g_L, \tag{45}$$

where the definition of the filter in Eq. (43) requires that the excitatory conductance be normalized by the leak conductance here. Equation (45) can of course also be arrived at by inverse Fourier transforming the product $\tilde{A}_e(\omega)\tilde{g}_{e1}(\omega)/g_L$. The application of this filter equation is demonstrated in Fig. 2(E). Sags and rebounds in response to the square-pulse conductances are seen, which is indicative of voltage-activated currents that provide negative feedback.

E. Response to modulation in the suprathreshold regime

The firing-rate response shown in Fig. 2(C) is for that of a neuron in a fluctuation-driven firing regime (with $E_{s0}=-30$ mV and $\sigma=4$ mV). The range of steady-state firing rates shown in Fig. 1(E) also covers neurons in the suprathreshold regime (for $E_{s0}>-25.5$ mV). It is worth noting that the firing-rate response in the suprathreshold regime is markedly different [7] from the fluctuation driven case: in the low-noise quasideterministic case the intrinsic firing-rate resonance arising from the gated current is suppressed and new firing-rate resonances appear at frequencies equivalent to the steady-state rate r_0 and its harmonics (this is also seen

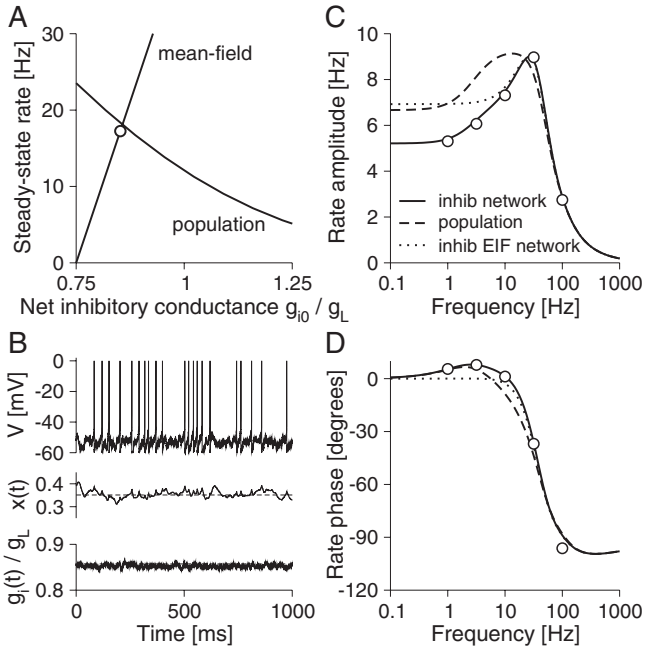

FIG. 3. A recurrent network of inhibitory GEM neurons with voltage-activated currents. (A) Construction for finding the steady-state network rate r_0 (for an example $g^a_{e0}=1.14g_L$ and $g^a_{i0}=0.75g_L$). Network rate and combined inhibitory conductance g_{i0} are found at the intersection of the population rate curve parametrized by g_{i0} [Eqs. (15) and (16)] and the mean-field rate curve [Eq. (48)]. The intersection agrees well with the rate (circle symbol) from a simulation of the recurrent network. (B) Simulated voltage and gating variables for a neuron in the network as well as the combined inhibition. Dashed lines are the theoretical predictions for x_0 and g_{i0}. (C) The amplitude and (D) the phase of the firing-rate modulation $\hat{r}_1$ [bold line, Eq. (56); symbols, simulations] for a modulated excitatory conductance $\hat{g}^a_{e1}=0.057g_L$. Rate modulation for a population [dashed line, Eq. (56) with $\hat{\gamma}_{i1}=0$; see Fig. 2(C)] and an inhibitory network of neurons without voltage-activated currents [dotted line, Eq. (56) with $\gamma_x=0$] are also plotted for comparison. The network coupling $c_i=0.59g_L$ and fluctuations $\sigma=4$ mV were chosen to give a steady state equivalent to that in Fig. 1.

in neurons without subthreshold currents [25]). For example, in the GEM neuron the firing-rate response for $E_{s0}=-20$ mV and $\sigma=4$ mV would show a resonance at ~ 80 Hz, a frequency close to the steady-state rate seen in Fig. 1(E). These two distinct mechanisms for firing-rate resonances appear to be mutually exclusive, with the fluctuation strength determining which manifests itself in the rate response [7].

V. SYNAPTICALLY COUPLED RECURRENT NETWORKS

The results of the previous section for uncoupled populations of neurons may be used to address the case of recurrently coupled networks in the mean-field (all-to-all coupling) approximation. This is achieved by allowing the incoming synaptic drive to be a function of the spike rate of the network and then solving self-consistently [21,26–28].

To illustrate the method for neurons with voltage-activated currents, an inhibitory network will be considered that receives dynamic excitatory $g^a_e(t)$ and steady inhibitory g^a_{i0} afferent synaptic input as well as recurrent inhibitory synaptic drive $g^r_i(t)$ that is a function of the network firing-rate history

$$\tau_i \frac{dg^r_i}{dt} = \tau_i c_i r(t-\tau_d) - g^r_i. \tag{46}$$

Here $\tau_i=10$ ms is the GABAa filter constant, c_i measures the strength of the recurrent inhibitory conductance, $r(t)$ is the instantaneous firing rate averaged over all neurons in the network, and $\tau_d=2$ ms is the axonal delay.

Oscillations in the afferent excitatory synaptic conductance will be considered $g^a_e=g_{e0}+\hat{g}_{e1}e^{i\omega t}$ which will lead to a modulation $r(t)=r_0+\hat{r}_1 e^{i\omega t}$ in the firing rate. This in turn, via Eq. (46), will cause a modulation of the recurrent inhibitory synaptic drive $g^r_i(t)=g^r_{i0}+\hat{g}^r_{i1}e^{i\omega t}$, where

$$g^r_{i0}=c_i r_0 \tau_i \quad \hat{g}^r_{i1}=c_i \frac{e^{-i\omega\tau_d}}{1+i\omega\tau_i}\hat{r}_1\tau_i. \tag{47}$$

The combined steady-state component of the inhibitory drive is therefore

$$g_{i0}=g^a_{i0}+c_i r_0 \tau_i, \tag{48}$$

whereas the modulated component in this example stems only from the recurrency $\hat{g}_{i1}=\hat{g}^r_{i1}$.

A. Steady state of a recurrent network

The steady-state properties of a mean-field network of neurons with voltage-activated currents are found by extending the standard approach [21,26–28] in which the network steady state is linked to an equivalent population with an effective afferent drive that incorporates the recurrent component.

The method involves first finding a range of solutions for the steady-state firing rate r_0 of a population of uncoupled neurons receiving the fixed afferent excitatory input $g^a_{e0}=g_{e0}$ but with the level of combined inhibition g_{i0} varied. An example of a rate-versus-inhibitory-conductance curve is provided in Fig. 3(A). A second equation linking g_{i0} to the steady-state network firing rate r_0 can be found by rearranging Eq. (48) to yield $r_0=(g_{i0}-g^a_{i0})/c_i\tau_i$. This line is also plotted in Fig. 3(A). The intersection of the two curves gives the self-consistent network rate r_0 and, from Eq. (48), the level of the recurrent component of the steady-state inhibitory conductance. Figure 3(B) shows good agreement between the steady-state approximation x_0 and a simulation taken from a single neuron in the network. It can be noted that a particular choice $c_i=0.59g_L$ for the recurrent coupling strength has been made that leads to a network with a firing rate identical to the uncoupled population case in Figs. 1 and 2. This will allow for a comparison of the dynamical effects arising from recurrent network coupling and voltage-activated currents in the network.

B. Dynamics of a recurrent network

The derivation of the response of networks of EIF neurons to oscillatory synaptic drive [20] can be straightfor-

wardly generalized to include voltage-gated currents. Once the steady-state properties are known, the modulated flux $\hat{J}_1$ and the probability density $\hat{P}_1$ can be found by generalizing Eqs. (27) and (28) to the recurrent network case

$$-\frac{\partial \hat{J}_1}{\partial V} = i\omega \hat{P}_1 + \hat{r}_1[\delta(V - V_{th}) - \delta(V - V_{re})], \tag{49}$$

$$-\frac{\partial \hat{P}_1}{\partial V} = \frac{I_0}{g_L\sigma^2}\hat{P}_1 + \frac{C}{g_L\sigma^2}\hat{J}_1 + \frac{g_x\hat{x}_1}{g_L}\frac{(V-E_x)}{\sigma^2}P_0 + \frac{\hat{g}_{e1}}{g_L}\frac{(V-E_e)}{\sigma^2}P_0 + \frac{c_i e^{-i\omega\tau_d}\hat{r}_1\tau_i}{g_L(1+i\omega\tau_1)}\frac{(V-E_i)}{\sigma^2}P_0, \tag{50}$$

where P_0 is the steady-state network density found using the self-consistent combined inhibitory conductance g_{i0} in the solution to equation set (15) and (16). The modulated probability density, flux, and firing rate are again resolved into three components corresponding to the three inhomogeneous terms in Eq. (50)

$$\hat{P}_1 = \gamma_x\hat{x}_1\hat{P}_x + \hat{\gamma}_{i1}\hat{r}_1\tau_i\hat{P}_i + \hat{\gamma}_{e1}\hat{P}_e, \tag{51}$$

where $\hat{\gamma}_{i1}=(c_i/g_L)e^{-i\omega\tau_d}/(1+i\omega\tau_i)$. The modulated probability densities, fluxes, and rates $\hat{P}_x,\hat{J}_x,\hat{r}_x$ and $\hat{P}_e,\hat{J}_e,\hat{r}_e$ are identical to those calculated using Eqs. (29)–(37) for the population case. The additional quantities $\hat{P}_i$, $\hat{J}_i$, and $\hat{r}_i$ are found similarly by setting E_μ to the reversal potential for inhibition E_i. Once these terms are extracted using the threshold integration method, the modulated quantities required for the self-consistent calculation of $\hat{x}_1$ in Eq. (24) can be written as

$$\langle x_\infty/\tau_x\rangle_1 = \gamma_x\hat{x}_1\langle x_\infty/\tau_x\rangle_x + \hat{\gamma}_{i1}\hat{r}_1\tau_i\langle x_\infty/\tau_x\rangle_i + \hat{\gamma}_{e1}\langle x_\infty/\tau_x\rangle_e, \tag{52}$$

$$\langle 1/\tau_x\rangle_1 = \gamma_x\hat{x}_1\langle 1/\tau_x\rangle_x + \hat{\gamma}_{i1}\hat{r}_1\tau_i\langle 1/\tau_x\rangle_i + \hat{\gamma}_{e1}\langle 1/\tau_x\rangle_e. \tag{53}$$

From these equations $\hat{x}_1$ can be found in terms of $\hat{r}_1$,

$$\hat{x}_1 = \hat{\gamma}_{i1}\hat{r}_1\tau_i\hat{x}_{i1} + \hat{\gamma}_{e1}\hat{x}_{e1}, \tag{54}$$

where $\hat{x}_{e1}$ is given in Eq. (42) and where $\hat{x}_{i1}$ is the inhibitory analog with subscripts changed from $e\to i$. Finally, this form for $\hat{x}_1$ is substituted into the relation for the firing-rate modulation corresponding to Eq. (51)

$$\hat{r}_1 = \gamma_x\hat{x}_1\hat{r}_x + \hat{\gamma}_{i1}\hat{r}_1\tau_i\hat{r}_i + \hat{\gamma}_{e1}\hat{r}_e, \tag{55}$$

which can be solved for $\hat{r}_1$ to yield the modulation of the network rate

$$\hat{r}_1 = \hat{\gamma}_{e1}\frac{\hat{r}_e + \gamma_x\hat{x}_{e1}\hat{r}_x}{1-\hat{\gamma}_{i1}(\hat{r}_i\tau_i + \gamma_x\hat{x}_{i1}\hat{r}_x\tau_i)}, \tag{56}$$

where all quantities on the RHS excepting $\hat{\gamma}_{e1},\gamma_x,\tau_i$ are functions of frequency ω. An example of the frequency-dependent response properties of a network of inhibitory neurons with voltage-activated currents is shown in Figs. 3(C) and 3(D). The case of an uncoupled population of neurons [dashed lines, Eq. (56) with $\hat{\gamma}_{i1}=0$] and an inhibitory network of neurons without voltage-activated currents [dotted lines, Eq. (56) with $\gamma_x=0$] are also plotted. Both cases exhibit a firing-rate resonance stemming from two distinct negative-feedback mechanisms: the voltage-activated current and the recurrent inhibition. It is interesting to note that here these two effects combine in the complete network to produce a more profound firing-rate resonance.

C. Multiple gating variables

The biophysical models to be treated in the next section feature more than one gating variable, requiring a minor extension of the methodology developed for the one gating-variable model of Sec. II. Consider a model with two ionic currents $g_x x(V-E_x)+g_y y(V-E_y)$ with gating-variable dynamics of the form in Eq. (8). For multiple gating variables, the steady-state values x_0 and y_0 are best found using a damped iterative approach where, starting from some initial values $x_0^{in(1)}$ and $y_0^{in(1)}$, the density $P_0(V;x_0^{in(1)},y_0^{in(1)})$ is derived and used to obtain new estimates $x_0^{in(2)},y_0^{in(2)}$ via equations of forms (11) and (19).

Once the steady state is found, the modulations $\hat{x}_1$ and $\hat{y}_1$ follow the form of Eq. (24) but with the average over $\hat{P}_1$ now including contributions from both gating variables. Hence, the two-variable generalizations of the modulated current (38) and density (39) equations are

$$\hat{r}_1 = \gamma_x\hat{x}_1\hat{r}_x + \gamma_y\hat{y}_1\hat{r}_y + \hat{\gamma}_{e1}\hat{r}_e, \tag{57}$$

$$\hat{P}_1 = \gamma_x\hat{x}_1\hat{P}_x + \gamma_y\hat{y}_1\hat{P}_y + \hat{\gamma}_{e1}\hat{P}_e, \tag{58}$$

where the contributions $\hat{P}_x,\hat{P}_y,\hat{P}_e$ and the corresponding rate modulations $\hat{r}_x,\hat{r}_y,\hat{r}_e$ are found exactly as for the one-variable case [Eqs. (29) and (30)]. The forms required for $\hat{x}_1$ of Eq. (24) are now

$$\langle x_\infty/\tau_x\rangle_1 = \gamma_x\hat{x}_1\langle x_\infty/\tau_x\rangle_x + \gamma_y\hat{y}_1\langle x_\infty/\tau_x\rangle_y + \hat{\gamma}_{e1}\langle x_\infty/\tau_x\rangle_e \tag{59}$$

and similarly for $\langle 1/\tau_x\rangle_1$. Substituting this into Eq. (24) and performing an identical procedure for y yields two simultaneous linear equations:

$$\hat{x}_1 = \hat{\gamma}_{e1}\hat{x}_{e1} + \gamma_y\hat{y}_1\hat{x}_{y1}, \tag{60}$$

$$\hat{y}_1 = \hat{\gamma}_{e1}\hat{y}_{e1} + \gamma_x\hat{x}_1\hat{y}_{x1}, \tag{61}$$

where the terms $\hat{x}_{e1}$, $\hat{x}_{y1}$, etc. are identical in form to Eq. (42) but with appropriate changes to subscripts. The equation pair (60) and (61) can then be solved to yield

$$\hat{x}_1 = \hat{\gamma}_{e1}\frac{\hat{x}_{e1} + \gamma_y\hat{x}_{y1}\hat{y}_{e1}}{1-\gamma_x\gamma_y\hat{x}_{y1}\hat{y}_{x1}}, \tag{62}$$

$$\hat{y}_1 = \hat{\gamma}_{e1}\frac{\hat{y}_{e1} + \gamma_x\hat{y}_{x1}\hat{x}_{e1}}{1-\gamma_x\gamma_y\hat{x}_{y1}\hat{y}_{x1}}, \tag{63}$$

from which the modulated rate and the probability density in Eqs. (57) and (58) are found.

VI. TWO BIOPHYSICAL EXAMPLES

The methods will now be applied to two biophysical models. The first is an entorhinal cortex layer-II neuron model,

adapted from Refs. [29–31] and comprises a two-variable I_h current and a noninactivating persistent sodium current. The second is a Traub-Miles model of a neuron with spike-frequency adaptation, modified from [9,32,33], which features two high-threshold potassium currents: the voltage-dependent I_M and the calcium-dependent I_{mAHP}. Before applying the method to these models, the effect of a spike shape is addressed.

A. Spike shape and refractoriness

Until now the spike was modeled as an exponential runoff to a threshold V_{th} followed by an abrupt reset to V_{re}. This reset discontinuity could potentially lead to inaccuracies in the modeling of currents that have shorter time constants at high voltages. Furthermore, high-threshold activated currents, like the spike-frequency adaptation of the Traub-Miles model, are strongly dependent on the shape of the spike and an explicit form for the downswing and the refractory period is required.

The methodology so far developed can be readily extended to include any deterministic spike shape, starting from a threshold V_{th} (that need not to be at the spike peak) and bringing the voltage around to a final reset V_{re} (potentially including a subthreshold refractory period) from which the stochastic dynamics continue. How the method can be extended to include a spike shape is described in detail in Appendix B. For the two biophysically detailed models treated here, a simple spike dynamics is chosen: a linear repolarization from the spike peak at V_{th} to a reset V_{re} [see Eq. (B3)]. This choice is a fair approximation of the downswing in many continuous-spike models. The height of the threshold and the width of the spike were chosen to ensure that the voltage-impulse delivered to the voltage-activated currents is the same as for the original models [9,29–33] that featured continuous Hodgkin-Huxley-like spike dynamics.

B. Entorhinal cortex layer-II neuron

The model, adapted from Refs. [29–31], features a persistent sodium current I_P and a mixed-cation current I_h,

$$C\frac{dV}{dt} + I_L + I_{spike} + I_P + I_h = I_{syn}. \tag{64}$$

The action potential has the upswing given by I_{spike} of Eq. (6) up until the threshold V_{th}, which is followed by a deterministic linear voltage downswing to the reset V_{re} from which the stochastic voltage-dynamics continue (see Appendix B). The leak I_L and the synaptic I_{syn} currents are of the form described in Sec. II.

The persistent sodium current described in [29] has an instantaneous activation $p_\infty(V)$ as well as a very slow inactivation of time scale >1 s, the latter of which is not included here, so that

$$I_P = g_P p_\infty (V - E_{\mathrm{Na}}). \tag{65}$$

The persistent sodium current is therefore approximated by a static nonlinearity and does not feature a gating variable that would require approximation using the self-consistent approach. The I_h current has two independent gating variables: one fast $f(t)$ and the other slow $s(t)$

$$I_h = (g_f f + g_s s)(V - E_h) \tag{66}$$

with conductances in the ratio $g_f/g_s = 1.85$. The variables follow the voltage-dependent dynamics of Eq. (8) with all additional parameters provided in Appendix C.

The results of the method applied to this model are shown in Figs. 4(A)–4(F). The negative feedback provided by the largely subthreshold I_h current, and boosted by the fast positive feedback of the I_P current, leads to a firing-rate resonance as seen in Fig. 4(D). The real-time filter [Fig. 4(E)] applied to a patterned excitatory conductance leads to a weak sag-rebound response to abrupt changes in the presynaptic rate [Fig. 4(F)].

C. Traub-Miles model of an adapting neuron

The modified Traub-Miles model [9,32,33] has two potassium currents that lead to spike-frequency adaptation: a voltage-dependent I_M and a calcium-dependent I_{mAHP},

$$C\frac{dV}{dt} + I_L + I_{spike} + I_M + I_{\mathrm{Ca}} + I_{mAHP} = I_{syn}. \tag{67}$$

The spike is again modeled as an exponential rise to threshold [Eq. (6)] followed by a linear downswing to reset (see Appendix B). The leak I_L and the synaptic I_{syn} currents are of the form described in Sec. II.

The voltage-activated potassium current is written as

$$I_M = g_M w (V - E_K) \tag{68}$$

and features a gating variable $w(t)$ with the dynamics of Eq. (8). The calcium current is modeled with an instantaneous activation $s_\infty(V)$,

$$I_{\mathrm{Ca}} = g_{\mathrm{Ca}} s_\infty (V - E_{\mathrm{Ca}}) \tag{69}$$

and the related medium-after-hyperpolarization current I_{mAHP} takes the form

$$I_{mAHP} = g_{mAHP}\frac{[\mathrm{Ca}^{2+}]}{30 + [\mathrm{Ca}^{2+}]}(V - E_K), \tag{70}$$

where $[\mathrm{Ca}^{2+}]$ is the time-dependent intracellular calcium concentration. The dynamics of $[\mathrm{Ca}^{2+}]$ follows

$$\tau_{\mathrm{Ca}}\frac{d[\mathrm{Ca}^{2+}]}{dt} = -0.16 I_{\mathrm{Ca}}(V) - [\mathrm{Ca}^{2+}] \tag{71}$$

and is of form (8) with $[\mathrm{Ca}^{2+}]_\infty = -0.16 I_{\mathrm{Ca}}(V)$. It can therefore be treated in the framework of voltage-gated currents. The only minor complication is that the prefactor of the voltage term in Eq. (70) is nonlinear in $[\mathrm{Ca}^{2+}]$ and so, for the steady-state approximation, for example, the prefactor will be replaced with $[\mathrm{Ca}^{2+}]_0/(30+[\mathrm{Ca}^{2+}]_0)$, where $[\mathrm{Ca}^{2+}]_0$ is calculated from the probability density in the way described previously for the cases of many gating variables.

The modulatory response proceeds similarly with Eq. (30) for $\mu = [\mathrm{Ca}^{2+}]$ being replaced with

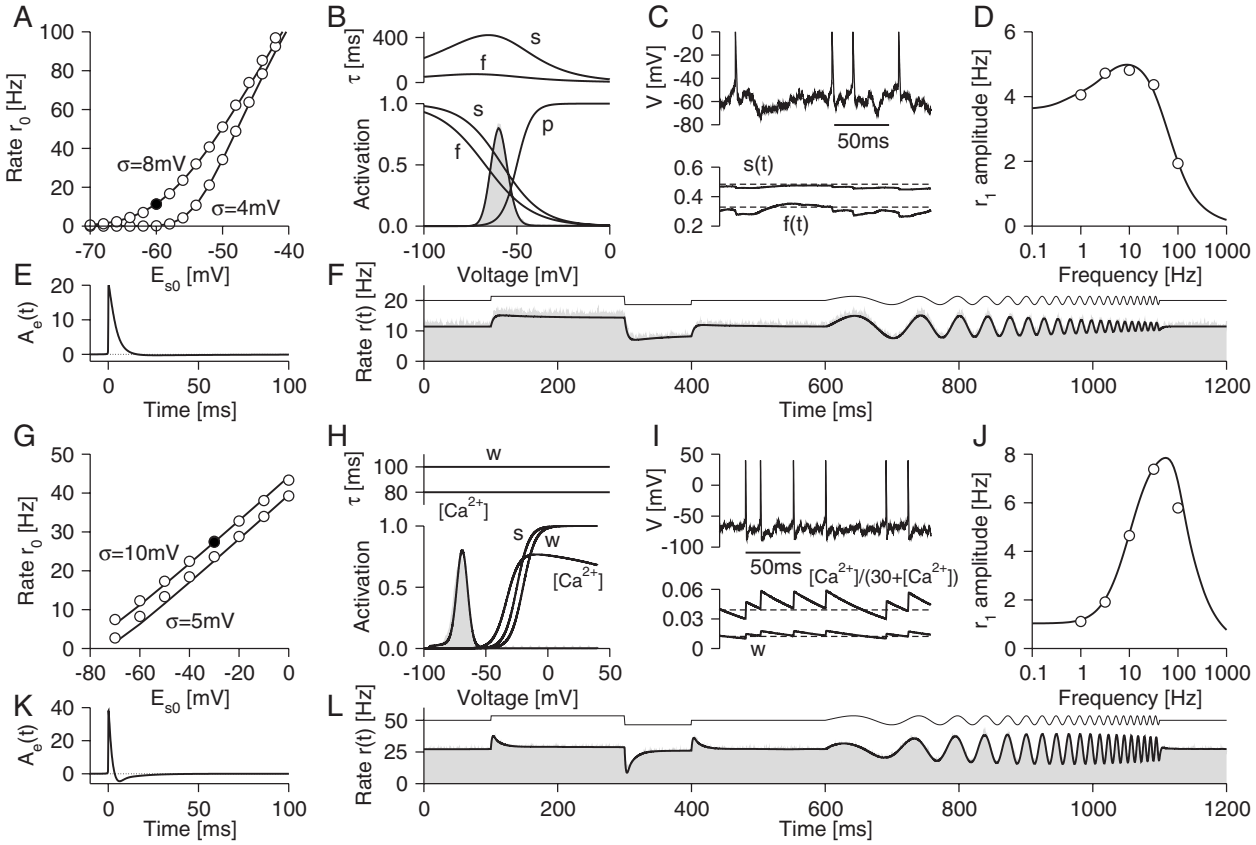

FIG. 4. Two biophysical models. (A)–(F) Entorhinal cortex layer-II neuron with persistent sodium and I_h currents. (A) Steady-state rate as a function of synaptic potential E_{s0} (with $g_{s0}=2g_L$) for two fluctuation strengths (lines, theory; symbols, simulations). (B) Voltage dependence of time constants and activation plotted with the steady-state density P_0 (line, theory; gray histogram, simulation) for the case $E_{s0}=-60$ mV, $g_{e0}=0.29g_L$, $g_{i0}=1.71g_L$, and $\sigma=8$ mV [filled symbol in panel (A)]. (C) Voltage and gating-variable time courses for the same case (dashed lines, steady-state approximations s_0, f_0). (D) Firing-rate response to modulated excitatory synaptic conductance ($g_{e1}=0.057g_L$) for the example, showing a resonance near 10 Hz. (E) Real-time filter corresponding to the inverse Fourier transform of panel (D). A weak undershoot is perceptible. (F) Response to patterned excitatory stimulus [thin line, with $g_{e1}(t)/g_L$ three times that of Fig. 2(E)] showing good agreement between theory (bold line) and simulation (gray histogram). (G)–(L) Modified Traub-Miles neuron with voltage-activated I_M and calcium-activated I_{mAHP} potassium currents. (G) Steady-state voltage as a function of E_{s0} (with $g_{s0}=2g_L$) for two fluctuation strengths. (H) Time constants and activation profiles with the steady-state density P_0 for the case $E_{s0}=-30$ mV, $g_{e0}=1.14g_L$, $g_{i0}=0.86g_L$, and $\sigma=10$ mV [filled symbol in panel (G)]. (I) Voltage and gating-variable time courses for the same case (dashed lines, steady-state approximations $w_0, [\mathrm{Ca}^{2+}]_0/(30+[\mathrm{Ca}^{2+}]_0)$). (J) Firing-rate response to modulated excitatory synaptic conductance ($g_{e1}=0.057g_L$) for this case, showing a pronounced resonance near 40 Hz. (K) Corresponding real-time filter exhibiting a visible undershoot. (L) Response to a patterned excitatory stimulus [$g_{e1}(t)/g_L$ 1.5 times that of Fig. 2(E)]. All other model parameters can be found in Appendix B and C.

$$-\frac{\partial \hat{P}_{\mathrm{Ca}^{2+}}}{\partial V}=\frac{I_0}{g_L\sigma^2}\hat{P}_{\mathrm{Ca}^{2+}}+\frac{C}{g_L\sigma^2}\hat{J}_{\mathrm{Ca}^{2+}}+\frac{30}{([\mathrm{Ca}^{2+}]_0+30)^2}\frac{(V-E_{\mathrm{Ca}})}{\sigma^2}P_0, \tag{72}$$

where the differential of the gating prefactor of Eq. (70) has been used. (It should be noted that for the case of a spike shape the corresponding equation involves the replacement $P_0 \to p_0 r_0$; see Appendix B for further details). The modulated probability density may then be written as the sum

$$\hat{P}_1=\gamma_M\hat{w}_1\hat{P}_w+\gamma_{mAHP}[\hat{\mathrm{Ca}}^{2+}]_1\hat{P}_{\mathrm{Ca}^{2+}}+\hat{\gamma}_{e1}\hat{P}_e \tag{73}$$

and similarly for $\hat{r}_1$ (where $\gamma_M=g_M/g_L$ and $\gamma_{mAHP}=g_{mAHP}/g_L$).

A comparison of the slow-gating variable approximation with simulations is provided in Figs. 4(G)–4(L). In Fig. 4(G) it can be seen that the approximation for the steady-state rate r_0 becomes accurate for $r_0>20$ Hz (see the Discussion). As is seen in Fig. 4(I) the deviations from the constant-gating-variable approximation can be significant for a low-rate case. The negative feedback from the spike-frequency adaptation produces a profound firing-rate resonance near 40 Hz [Fig. 4(J)], which is reflected in an undershoot in the real-time filter. These filtering properties lead to a response to patterned excitatory drive [Fig. 4(L)] that strongly accentuates transients.

VII. DISCUSSION

A generalized exponential integrate-and-fire model (GEM) was introduced that combines an explicit spiking

mechanism with nonlinear voltage-activated or calcium-activated transmembrane current. The framework differs substantially from traditional Hodgkin-Huxley-type models only in that the spike dynamics are discontinuous at some level. It is this discontinuity that is the key differentiator between the Hodgkin-Huxley-type and the integrate-and-fire-type models; both can incorporate conductance-based transmembrane currents.

Like other few-variable reduced neuron models, populations and networks of GEMs may be efficiently simulated on a computer, particularly if the nonlinear quantities are precalculated over the required voltage range and lookup tables are used during the simulation. This is also the case for Hodgkin-Huxley-type models with continuous spikes. However, in this paper it was further shown that many important quantities that characterize the dynamics of networks of GEMs can be obtained by using the threshold integration method. These included the firing-rate response curves, which are required for the stability analysis of network states, as well as the filters that give the first-order response of recurrent networks to patterned afferent drive. The framework readily generalizes to the treatment of networks comprising multiple neuron types. It should therefore greatly facilitate the analysis of how neuron-specific current-expression profiles contribute to activity seen at the tissue level.

Limitations and extensions of the method

The method relies on a separation of time scales between the gating kinetics and the underlying voltage dynamics, a method that has been previously employed with leaky or perfect-integrator IF models coupled to second variables [7,8,11]. The approximation is a good one for biologically relevant cases, as shown in Fig. 4, and becomes increasingly accurate under naturalistic conditions of high synaptic conductance in which the voltage time constant can become significantly reduced.

In the context of adaptation, however, it is the spike period that should be small compared to the dynamics of the additional variables. Given that the typical channel kinetics are on a time scale on the order of 50–100 ms [9] this requires rather high rates ($\gg 20$ Hz) for the slow-time-constant approach to become accurate. The case of $r_0 \sim 27$ Hz was chosen for Figs. 4(G)–4(L) and demonstrate a good agreement, but it can be seen at lower rates that the theoretical results systematically underestimate the simulated firing rate. This is due to the validity of the constant gating variable approximation in this case [see Fig. 4(I)] and is a general problem for any theoretical approach that replaces fluctuating spike-triggered currents with an average value. However, because the method here is equivalent to the first-order solution to an expansion of the full high-dimensional Fokker-Planck equation (see Ref. [34] for a similar scenario), it would be possible to systematically improve upon the method by calculating the results to higher order. This would allow quantitative predictions for the role of adaptation in the physiologically relevant limit of low firing rates.

Currents with kinetics faster than the voltage dynamics can also be incorporated into the GEM framework, but the present study did not consider these cases theoretically. Two biophysical features that were neglected, and that give rise to fast kinetics, are the filtered synaptic fluctuations and the sodium-current inactivation. First, a perturbative method for accounting for the effects of synaptic AMPA kinetics on the firing rate of quadratic IF neurons has already been developed [34]. The general observation was that, unlike for the leaky IF case with a low spike threshold, the transition from white to colored noise for nonlinear IF models does not produce qualitatively new scaling behavior, at least for the high-frequency response. Nevertheless, it would be worth repeating the analysis of Ref. [34] for the EIF so as to derive the corresponding analytical forms for the firing rate and the probability density. Second, the case of sodium-current inactivation (the Hodgkin-Huxley h gating variable) does not yet appear to have been treated analytically in the context of stochastic voltage dynamics. It has already been identified as a source for the variability of the spike threshold [35] in different classes of neurons. The development of a tractable model of this mechanism would considerably increase our understanding of the response properties of neurons in the region of action-potential generation.

ACKNOWLEDGMENTS

M.J.E.R. acknowledges support from the Research Councils United Kingdom. Nicolas Brunel and Vincent Hakim are warmly thanked for many useful discussions.

APPENDIX A

1. Threshold integration method

Threshold integration [19,20] provides a direct route to numerical solutions of the Fokker-Planck equations that describe integrate-and-fire neurons. The method splits the second-order Fokker-Planck equation into two first-order equations for the probability flux and density which, after scaling, may be solved by integrating from the voltage threshold V_{th} to some lower bound V_{lb}. The advantage of the method comes from the fact that the boundary conditions at threshold and reset are automatically accounted for. In this section the method will be described in detail, but please note that all code used in this paper is freely available from the author.

The voltage range is discretized into steps Δ, so that $V^{(k)}=V_{lb}+k\Delta$ and $V_{th}=V^{(n)}=V_{lb}+n\Delta$. Here the lower bound V_{lb} is chosen, so that the probability of finding a neuron with a voltage near V_{lb} is vanishingly small (typically $V_{lb}=-100$ mV). It is also convenient to choose the step size Δ, so that the reset voltage V_{re} falls on a lattice point $V_{re}=V_{lb}+k_{re}\Delta$, where k_{re} is an integer.

Before going on to describe the method, an integration algorithm with good convergence properties is first provided. Both steady-state and modulatory cases involve integrating equations for probability densities that are of the form

$$-\frac{dP}{dV}=GP+H, \tag{A1}$$

where G and H are functions of voltage and where H includes terms proportional to the flux and potentially the

steady-state density [see, for example, Eqs. (16), (33), and (35)]. For the EIF model G contains terms that are exponentially large for $V>V_T$ and so a naive forward-Euler scheme would require a correspondingly small Δ for good convergence. For this reason it proves useful to first solve Eq. (A1) for P in terms of G and H between $V^{(k)}$ and $V^{(k-1)}$ as follows:

$$P^{(k-1)} = P^{(k)} \exp\left(\int_{V^{(k-1)}}^{V^{(k)}} G dV \right) + \int_{V^{(k-1)}}^{V^{(k)}} dV\, H \exp\left(\int_{V^{(k-1)}}^{V} G dV' \right) \tag{A2}$$

$$= P^{(k)} \alpha^{(k)} + \Delta H^{(k)} \beta^{(k)} \tag{A3}$$

plus corrections of order Δ^2 and where

$$\alpha^{(k)} = e^{\Delta G^{(k)}}, \quad \beta^{(k)} = \frac{e^{\Delta G^{(k)}} - 1}{\Delta G^{(k)}}. \tag{A4}$$

Equation (A3) is the integration scheme used throughout this paper for the integration of probability densities backward from threshold. Finally, as a minor technical point for numerical implementations, it should be noted that for certain parameter choices it is possible that $G^{(k)}=0$ at some k. In this case the numerator and the denominator of $\beta^{(k)}$ vanish and $\beta^{(k)}=1$.

2. Threshold integration for the steady state

The discretized equations (15) and (16) are integrated backward from threshold V_{th} where $k=n$ to the lower bound V_{lb} where $k=0$ with the boundary conditions at threshold being $j_0^{(n)}=1$ and $p_0^{(n)}=0$,

$$j_0^{(k-1)} = j_0^{(k)} - \delta_{k,k_{re+1}}, \tag{A5}$$

$$p_0^{(k-1)} = p_0^{(k)} \alpha^{(k)} + \Delta \frac{C j_0^{(k)}}{g_L \sigma^2} \beta^{(k)}. \tag{A6}$$

The Kronecker delta $\delta_{j,k}$ takes the value $\delta_{j,k}=1$ if $j=k$ and is zero otherwise. After integration of j_0 and p_0 from V_{th} to V_{lb}, the steady-state rate is recovered from the condition $r_0 = 1/\Sigma_{k=1}^{n} \Delta p_0^{(k)}$, which in turn yields the correctly normalized density $P_0=r_0 p_0$.

3. Threshold integration for modulations

To obtain the functions $\hat{J}_\mu$ and $\hat{P}_\mu$ that comprise the modulated response the solutions of two pairs of equations, Eqs. (32) and (33) and Eqs. (34) and (35), must be found. The first pair has threshold conditions $\hat{j}_\mu^{(n)}=0$ and $\hat{p}_\mu^{(n)}=0$ and discretized forms

$$\hat{J}_\mu^{(k-1)} = \hat{J}_\mu^{(k)} + \Delta i\omega \hat{p}_\mu^{(k)}, \tag{A7}$$

$$\hat{p}_\mu^{(k-1)} = \hat{p}_\mu^{(k)} \alpha^{(k)} + \Delta \frac{C \hat{J}_\mu^{(k)}}{g_L \sigma^2} \beta^{(k)} + \Delta \frac{C}{\sigma^2} (V - E_\mu) P_0^{(k)} \beta^{(k)}, \tag{A8}$$

where $P_0^{(k)}=r_0 p_0^{(k)}$ is the normalized steady-state density. For the second pair of equations, the initial conditions are $\hat{J}_\mu^{(n)}=1$ and $\hat{p}_\mu^{(n)}=0$ and the discretized forms are

$$\hat{J}_r^{(k-1)} = \hat{J}_r^{(k)} + \Delta i\omega \hat{p}_r^{(k)} - \delta_{k,k_{re+1}}, \tag{A9}$$

$$\hat{p}_r^{(k-1)} = \hat{p}_r^{(k)} \alpha^{(k)} + \Delta \frac{C}{g_L \sigma^2} \hat{J}_r^{(k)} \beta^{(k)}. \tag{A10}$$

These two pairs of equations are integrated from threshold to the lower bound and then the zero-flux condition in Eq. (37) is used to extract the modulated rate

$$\hat{r}_\mu = -\hat{J}_\mu^{(0)} / \hat{J}_r^{(0)}. \tag{A11}$$

This rate modulation then gives the flux $\hat{J}_\mu$ and probability-density $\hat{P}_\mu$ modulations via equation pair (31).

APPENDIX B

1. Spike shape and refractory period

The exponential IF model [12] improves upon the leaky IF model by incorporating the sodium-channel activation that initiates the spike. The potassium-mediated spike downswing is treated as a discontinuous reset from threshold V_{th} to V_{re}. A refractory period can be included, typically by waiting some fixed time between when the threshold is reached and when the dynamics eventually continues from the reset. For neurons without voltage-gated channels what the voltage does during the refractory period is irrelevant. However, in the presence of such currents the shape of the spike can have a significant impact on dynamics—particularly for high-threshold frequency-adaptation currents. It is now demonstrated, using the example model of Sec. II, how an explicit spike shape may be included into the formalism of EIF neurons with voltage-gated currents.

2. Discontinuous dynamics

It is assumed that neurons evolve under a stochastic dynamics until the spike threshold V_{th} is reached (this need not be the peak of the spike). From this point the dynamics becomes deterministic, following a fixed spike shape, and eventually bringing the neuronal voltage to the reset V_{re} after a time τ_{ref} has elapsed. Over this period any voltage-gated variables continue to respond to the voltage in the usual way. This "pasting on" of a voltage-spike template is in the spirit of the spike-response model formalism [36,37] and is quite general; the shape need not be monotonic in voltage but might, for example, start from the region of the spike where the initial exponential begins to be dominated by additional terms and the EIF approximation loses validity (see the experimental data in the inset of Fig. 2 in Ref. [15]). This

formalism will allow for accurate fits to experimentally measured spike dynamics.

For neurons with a spike shape the probability density $P(V,t)$ for the voltage will have two components:

$$P(V,t) = \varrho(V,t) + \varrho_{ref}(V,t), \tag{B1}$$

where $\varrho(V,t)$ is the density of active nonrefractory neurons (undergoing stochastic dynamics) and $\varrho_{ref}(V,t)$ is the density of those neurons that are currently refractory (on the deterministic component of the spike). The last contribution can be written in the form

$$\varrho_{ref}(V,t) = \int_0^{\tau_{ref}} ds\ r(t-s)\delta(V - V_{sp}(s)), \tag{B2}$$

where V_{sp} is the deterministic spike trajectory. Here, for reasons of clarity, a monotonic linear trajectory from threshold to reset will be used as an example,

$$V_{sp}(t) = V_{th} - \frac{t}{\tau_{ref}}(V_{th} - V_{re}), \tag{B3}$$

which provides a reasonable fit to the spike downswing of the Wang-Buszaki model [13].

3. Steady-state population of refractory neurons

The steady-state rate r_0 and the probability density P_0 for refractory neurons with voltage-gated currents can be related to the nonrefractory case with instantaneous reset treated in Secs. III–V. The average period for the refractory case is τ_{ref} longer than for the nonrefractory case because it includes the additional spike dynamics, and so

$$r_0 = \frac{1}{\int_{V_{lb}}^{V_{th}} p_0 dV + \tau_{ref}}, \tag{B4}$$

where p_0 is given by the solution of equation pair (15) and (16) with the (still unknown) steady-state gating x_0. As before, x_0 needs to be calculated self-consistently using the steady-state form of Eq. (B1) for the probability density

$$P_0 = r_0 p_0 + \frac{r_0 \tau_{ref}}{(V_{th} - V_{re})}\theta(V - V_{re}) \tag{B5}$$

for $V < V_{th}$, where $r_0 p_0 = \varrho_0$ is the density of active neurons [calculated from Eqs. (15) and (16)] and where the second term on the right-hand side in the above equation is the density of refractory neurons calculated from Eqs. (B2) and (B3) in the steady-state. This steady-state density (B5) is then calculated over a range of x_0 [which parametrizes the p_0 term in Eq. (B5)] until $x_0^{out} = x_0^{in}$ in relation (17) is satisfied. This yields the self-consistent gating x_0, the probability density P_0, and the firing rate r_0 for the steady-state refractory case. The steady-state rates and the probability density of a refractory neuron are shown in Figs. 5(A) and 5(B) together with a voltage time course in which the spike shape can be seen.

4. Modulatory response for the refractory case

The response to modulation for neurons with a spike shape requires some minor alterations to the corresponding

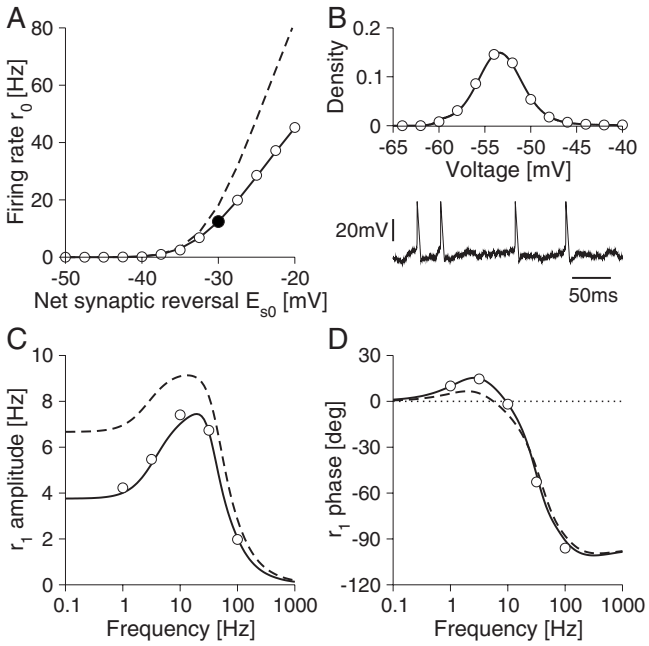

FIG. 5. A population of GEM neurons with spike shape [Eq. (B3)] of width $\tau_{ref}=5$ ms. (A) Steady-state rate as a function of excitatory-inhibitory balance E_{s0} with $\sigma=4$ mV and $g_{s0}=2g_L$ [bold line, theory; symbols, simulation; dashed line, nonrefractory case of Fig. 1(E)]. (B) Steady-state density when $E_{s0}=-30$ mV (bold line, theory; symbols, simulation). A voltage time course is shown below in which the spike shape is discernible. (C) The rate amplitude and (D) the phase in response to modulated excitatory conductance [bold line, theory; symbols, simulation; dashed line, nonrefractory case of Fig. 2(C)]. Apart from the spike shape, all other parameters are identical to the corresponding cases in Figs. 1 and 2.

nonrefractory response. Modulated excitatory synaptic conductance is again used as an example. From Eq. (B1) the first-order time-dependent probability density is resolved into active $\hat{\varrho}_1$ and refractory $\hat{\varrho}_{ref1}$ components. The active component can be found by separating it into densities related to modulations of the gating variable and the excitatory drive

$$\hat{r}_1 = \gamma_x \hat{x}_1 \hat{r}_x + \hat{\gamma}_{e1}\hat{r}_e, \tag{B6}$$

$$\hat{\varrho}_1 = \gamma_x \hat{x}_1 \hat{\varrho}_x + \hat{\gamma}_{e1}\hat{\varrho}_e. \tag{B7}$$

The quantities $\hat{\varrho}_\mu$ and $\hat{r}_\mu$ with $\mu = e,x$ have been previously derived in Ref. [20] and are the solutions to

$$-\frac{\partial \hat{J}_\mu}{\partial V} = i\omega\hat{\varrho}_\mu + \hat{r}_\mu[\delta(V - V_{th}) - e^{-i\omega\tau_{ref}}\delta(V - V_{re})], \tag{B8}$$

$$-\frac{\partial \hat{\varrho}_\mu}{\partial V} = \frac{I_0}{g_L\sigma^2}\hat{\varrho}_\mu + \frac{C}{g_L\sigma^2}\hat{J}_\mu + \frac{(V - E_\mu)}{\sigma^2}r_0 p_0, \tag{B9}$$

where it should be noted that the inhomogeneous term in Eq. (B9) is proportional to the steady-state density $r_0 p_0$ of the active neurons only. These equations are solved using a similar threshold integration method as in Eqs. (31)–(37) with the

probability density P_0 replaced with $r_0 p_0$ in Eq. (33) and with the delta function in Eq. (34) now multiplied by the factor $e^{-i\omega\tau_{ref}}$. The solutions of these equations yield all the quantities required for the firing-rate modulation $\hat{r}_1$ [Eq. (B6)] and the active component of the modulated probability density $\hat{\varrho}_1$ [Eq. (B7)] except that $\hat{x}_1$ still remains to be found. To extract this quantity requires the full probability density modulation $\hat{P}_1$. This will include the contribution from the deterministic component of the spike $\hat{\varrho}_{ref1} = \tau_{ref}\hat{r}_1\hat{\varrho}_{sp}$ where, for the postspike form in Eq. (B3),

$$\hat{\varrho}_{sp} = \frac{e^{-i\omega\tau_{ref}(V_{th}-V)/(V_{th}-V_{re})}}{(V_{th}-V_{re})}\theta(V-V_{re}) \tag{B10}$$

for $V < V_{th}$. Hence

$$\hat{P}_1 = \gamma_x\hat{x}_1\hat{\varrho}_x + \hat{\gamma}_{e1}\hat{\varrho}_e + \tau_{ref}\hat{r}_1\hat{\varrho}_{sp}. \tag{B11}$$

Substituting for $\hat{r}_1$ from Eq. (B6) into Eq. (B11) yields

$$\hat{P}_1 = \gamma_x\hat{x}_1\hat{P}_x + \hat{\gamma}_{e1}\hat{P}_e, \tag{B12}$$

where now

$$\hat{P}_\mu = \hat{\varrho}_\mu + \tau_{ref}\hat{r}_\mu\hat{\varrho}_{sp} \tag{B13}$$

for $\mu = e, x$. This redefinition of $\hat{P}_\mu$ for the refractory case brings the refractory modulated probability density (B12) into the same symbolic form as for the nonrefractory case [see Eq. (39)] and so Eq. (42) provides the modulation of the gating variable $\hat{x}_{e1}$ with the refractory $\hat{P}_\mu$'s [Eq. (B13)] used to calculated all terms except for the integral over the steady-state distribution (the $\langle 1/\tau_x\rangle_0$ term) for which Eq. (B5) is used. The resulting $\hat{x}_1$ gives the firing-rate modulation [Eq. (B6)] and subsequently allows for the full probability modulation in Eq. (B11) to be found.

Figure 5 shows the steady-state and response properties, generalized from Figs. 1(E) and 2(C), for a neuron with a spike shape. For this particular example the resonance is visibly more pronounced [Fig. 5(C)]. This is a direct consequence of the more detailed model of the spike (increased time spent at higher voltages) interacting with the depolarization-activated current.

5. Recurrent network for the refractory case

The network steady state for refractory neurons can be calculated self-consistently from the population result, just as was done for the nonrefractory case. The calculation of the network response to modulation for refractory neurons is marginally more involved but can again be written in terms of a modulated population. The firing-rate modulation and the probability density of neurons that are not currently refractory are

$$\hat{r}_1 = \gamma_x\hat{x}_1\hat{r}_x + \hat{\gamma}_{i1}\hat{r}_1\tau_i\hat{r}_i + \hat{\gamma}_{e1}\hat{r}_e, \tag{B14}$$

$$\hat{\varrho}_1 = \gamma_x\hat{x}_1\hat{\varrho}_x + \hat{\gamma}_{i1}\hat{r}_1\tau_i\hat{\varrho}_i + \hat{\gamma}_{e1}\hat{\varrho}_e, \tag{B15}$$

where $\hat{r}_\mu$ and $\hat{\varrho}_\mu$ (with $\mu = e, i, x$) are calculated from solutions to Eqs. (B8) and (B9). The full modulated probability density is

$$\hat{P}_1 = \gamma_x\hat{x}_1\hat{\varrho}_x + \hat{\gamma}_{i1}\hat{r}_1\tau_i\hat{\varrho}_i + \hat{\gamma}_{e1}\hat{\varrho}_e + \tau_{ref}\hat{r}_1\hat{\varrho}_{sp}, \tag{B16}$$

which on substitution of Eq. (B14) into the last term proportional to $\hat{\varrho}_{sp}$ yields

$$\hat{P}_1 = \gamma_x\hat{x}_1\hat{P}_x + \hat{\gamma}_{i1}\hat{r}_1\tau_i\hat{P}_i + \hat{\gamma}_{e1}\hat{P}_e. \tag{B17}$$

Again, as for the refractory population, the redefinition of $\hat{P}_\mu$ [Eq. (B13)] with $\mu = e, x, i$ is used. The equations have now been brought into a form identical to the nonrefractory case (51) and hence Eqs. (54)–(56) can be used (with the $\hat{P}_\mu$'s for neurons with a spike shape) to obtain the required $\hat{r}_1$.

APPENDIX C: MODEL PARAMETERS

1. One gating-variable GEM neuron

The model is defined in Eqs. (7) and (8) and features a depolarization-activated hyperpolarizing current.

Capacitance: $C = 1\ \mu\mathrm{F/cm^2}$.

Leak current: $g_L = 0.05\ \mathrm{mS/cm^2}$ and $E_L = -80\ \mathrm{mV}$.

Spike-generating current I_{spike}: this is of the EIF form with $\Delta_T = 2\ \mathrm{mV}$, $V_T = -53\ \mathrm{mV}$, $V_{re} = -60\ \mathrm{mV}$, and $V_{th} = 0\ \mathrm{mV}$. The reset is instantaneous for Figs. 1–3 whereas in Fig. 5 a spike shape [Eq. (B3)] with linear repolarization from threshold to reset was used with $\tau_{ref} = 5\ \mathrm{ms}$.

Voltage-activated current: $g_x = 2g_L$, $E_x = -80\ \mathrm{mV}$,

$$x_\infty = \frac{1}{1+\exp[-(V-V_x)/\Delta_x]}, \tag{C1}$$

$$\tau_x(V) = \tau_{x1} + \tau_{x2}\exp[-(V-V_\tau)^2/2\Delta_\tau^2], \tag{C2}$$

where $V_x = -50\ \mathrm{mV}$, $\Delta_x = 5\ \mathrm{mV}$, $\tau_{x1} = 50\ \mathrm{ms}$, $\tau_{x2} = 20\ \mathrm{ms}$, $V_\tau = -50\ \mathrm{mV}$, and $\Delta_\tau^2 = 30\ \mathrm{mV}^2$. The activation x_∞ and the time constant τ_x are plotted in Fig. 1(B).

2. Entorhinal cortex layer-II neuron

The model is adapted from Refs. [29,30] and features [see Eq. (64)] a two-variable voltage-activated I_h current and an instantaneously activated persistent sodium current.

Capacitance: $C = 1\ \mu\mathrm{F/cm^2}$.

Leak current: $g_L = 0.078\ \mathrm{mS/cm^2}$, $E_L = -80\ \mathrm{mV}$.

Spike-generating current I_{spike}: this is of the EIF form [Eq. (6)] with $\Delta_T = 2\ \mathrm{mV}$, $V_T = -53\ \mathrm{mV}$, $V_{re} = -60\ \mathrm{mV}$, and $V_{th} = 0\ \mathrm{mV}$. A spike shape is included [Eq. (B3)] with a linear repolarization from threshold to reset lasting $\tau_{ref} = 2\ \mathrm{ms}$.

Persistent sodium current I_P: $E_{\mathrm{Na}} = 87\ \mathrm{mV}$ and $g_P = 0.223g_L$. This current activates instantaneously with p_∞ of the form of Eq. (C1) with $V_p = -50\ \mathrm{mV}$ and $\Delta_p = 4\ \mathrm{mV}$.

I_h current: $E_h = -20\ \mathrm{mV}$, $g_f = 0.815g_L$, and $g_s = 0.441g_L$. The gating variables f and s for the I_h obey the dynamics given in Eq. (8). The equilibrium value $f_\infty = \alpha_f/(\alpha_f+\beta_f)$ and time constants $\tau_f = 1/(\alpha_f+\beta_f)$ for the fast component are defined through $\alpha, \beta = (aV+b)/(1-e^{(V+b/a)/k})$, where for α_f ($a = -2.89\times10^{-3}$, $b = -0.445$, $k = 24.02$) and for β_f ($a = 2.71\times10^{-2}$, $b = -1.024$, $k = -17.4$). The parameters for the slow component are defined similarly through α_s ($a = -3.18\times10^{-3}$, $b = -0.695$, $k = 26.72$) and β_s ($a = 2.16\times10^{-2}$;

$b=-1.065$; $k=-14.25$). The activation and the time constants are all plotted in Fig. 4(B).

3. Neuron with spike-frequency adaptation

The neuron is an adapted Traub-Miles model [9,32,33] featuring voltage-activated and calcium-activated spike-frequency adaptation currents given in Eq. (67).

Capacitance: $C=1\ \mu\mathrm{F/cm}^2$.

Leak current: $g_L=0.1\ \mathrm{mS/cm}^2$, $E_L=-67\ \mathrm{mV}$.

Spike-generating current I_{spike}: this is of the EIF form [Eq. (6)] with $\Delta_T=2$ mV, $V_T=-65$ mV, $V_{re}=-95$ mV, and $V_{th}=40$ mV. A spike shape is included [see Eq. (B3)] with a linear repolarization from threshold to reset lasting $\tau_{ref}=1$ ms. The spike shape of the reduced model was chosen, so that its effect on the adaptation currents was matched to the continuous-spike model [9].

I_M current: defined in Eq. (68) where $g_M=80g_L$ and $E_K=-100$ mV, with w obeying the dynamics of Eq. (8) with $\tau_w=100$ ms, and w_∞ of the form of Eq. (C1) with $V_w=-20$ mV and $\Delta_w=5$ mV.

Calcium current I_{Ca}: defined in Eq. (69) with $g_{\mathrm{Ca}}=50g_L$ and $E_{\mathrm{Ca}}=120$ mV. The gating variable has instantaneous activation s_∞ and is of the form of Eq. (C1) with $V_s=-25$ mV and $\Delta_s=5$ mV.

Medium-after-hyperpolarization current I_{mAHP}: Defined in Eq. (70) with $g_{mAHP}=40g_L$ and $E_K=-100$ mV. The activation dynamics for $[\mathrm{Ca}^{2+}]$ are found in Eq. (71) with $\tau_{\mathrm{Ca}}=80$ ms being the remaining parameter to be specified. The activation and time constants are all plotted in Fig. 4(H).

[1] R. FitzHugh, Bull. Math. Biophys. **17**, 257 (1955).
[2] J. Nagumo, S. Arimoto, and S. Yoshizawa, Proc. IRE **50**, 2061 (1962).
[3] V. I. Krinskii and Y. M. Kokoz, Biofizika **18**, 506 (1973).
[4] J. Rinzel, in *Models in Neurobiology*, Nonlinear Phenomena in Physics and Biology Vol. 75, edited by R. H. Enns, B. L. Jones, R. M. Miura, and S. S. Rangnekar (NATO Advanced Study Institute, Alberta, Canada, 1980), pp. 347–367.
[5] G. D. Smith, C. L. Cox, S. M. Sherman, and J. Rinzel, J. Neurophysiol. **83**, 588 (2000).
[6] E. M. Izhikevich, Neural Networks **14**, 883 (2001).
[7] M. J. E. Richardson, N. Brunel, and V. Hakim, J. Neurophysiol. **89**, 2538 (2003).
[8] N. Brunel, V. Hakim, and M. J. E. Richardson, Phys. Rev. E **67**, 051916 (2003).
[9] J. Benda and A. V. M. Herz, Neural Comput. **15**, 2523 (2003).
[10] G. Fuhrmann, H. Markram, and M. Tsodyks, J. Neurophysiol. **88**, 761 (2002).
[11] G. Gigante, M. Mattia, and P. Del Giudice, Phys. Rev. Lett. **98**, 148101 (2007).
[12] N. Fourcaud-Trocme, D. Hansel, C. van Vresswijk, and N. Brunel, J. Neurosci. **23**, 11628 (2003).
[13] X.-J. Wang and G. Buzsáki, J. Neurosci. **16**, 6402 (1996).
[14] A. L. Hodgkin and A. F. Huxley, J. Physiol. (London) **117**, 500 (1952).
[15] L. Badel, S. Lefort, R. Brette, C. C. H. Petersen, W. Gerstner, and M. J. E. Richardson, J. Neurophysiol. **99**, 656 (2008).
[16] L. Badel, S. Lefort, T. K. Berger, C. C. H. Petersen, W. Gerstner, and M. J. E. Richardson, Biol. Cybern. **99**, 361 (2008).
[17] E. M. Izhikevich, Neural Networks **15**, 1063 (2004).
[18] R. Brette and W. Gerstner, J. Neurophysiol. **94**, 3637 (2005).
[19] M. J. E. Richardson, Phys. Rev. E **76**, 021919 (2007).
[20] M. J. E. Richardson, Biol. Cybern. **99**, 381 (2008).
[21] N. Brunel and V. Hakim, Neural Comput. **11**, 1621 (1999).
[22] B. Lindner and L. Schimansky-Geier, Phys. Rev. Lett. **86**, 2934 (2001).
[23] G. Silberberg, M. Bethge, H. Markram, K. Pawelzik, and M. Tsodyks, J. Neurophysiol. **91**, 704 (2004).
[24] H. Risken, *The Fokker-Planck Equation* (Springer-Verlag, Berlin, 1996).
[25] B. W. Knight, J. Gen. Physiol. **59**, 734 (1972).
[26] B. W. Knight, Neural Comput. **12**, 473 (2000).
[27] P. E. Latham, B. J. Richmond, P. G. Nelson, and S. Nirenberg, J. Neurophysiol. **83**, 808 (2000).
[28] N. Brunel and X.-J. Wang, J. Neurophysiol. **90**, 415 (2003).
[29] J. Magistretti and A. Alsono, J. Gen. Physiol. **114**, 491 (1999).
[30] C. T. Dickson, J. Magistretti, M. H. Shalinsky, E. Fransén, M. E. Hasselmo, and A. Alonso, J. Neurophysiol. **83**, 2562 (2000).
[31] E. Fransén, A. A. Alonso, C. T. Dickson, J. Magistretti, and M. E. Hasselmo, Hippocampus **14**, 368 (2004).
[32] R. D. Traub and R. Miles, *Neuronal Networks of the Hippocampus* (Cambridge University Press, Cambridge, England, 1991).
[33] B. Ermentrout, Neural Comput. **10**, 1721 (1998).
[34] N. Brunel and P. E. Latham, Neural Comput. **15**, 2281 (2003).
[35] C. Koch, Ö. Bernander, and R. J. Douglas, J. Comput. Neurosci. **2**, 63 (1995).
[36] W. Gerstner, R. Ritz, and J. L. van Hemmen, Biol. Cybern. **69**, 503 (1993).
[37] W. Gerstner, Phys. Rev. E **51**, 738 (1995).